# Programmable Self-Assembly of Homo- or Hetero-Metallomacrocycles using 4-(1H-pyrazolyl-4-yl)pyridine

**Jin Tong,[a] Shu-Yan Yu,*[a] and Hui Li*[b]**

[a]Laboratory for Self-Assembly Chemistry, Department of Chemistry, Renmin University of China, Beijing, 100872, P. R. China

[b]School of Material Science and Engineering, East China University of Science and Technology, Shanghai 200237, P. R. China

## Table of Contents

# Supporting Information

**Materials:** All chemicals and solvents were of reagent grade and were purified according to conventional methods.[1]

**Instrumentation**: $^1$H NMR experiments were performed on a Bruker Avance DMX400 spectrometer using tetramethylsilane. ESI-MS measurements were performed with an FT-ICR-MS mass spectrometer.

**X-ray Structural Determinations:**

Data for **1** was collected at 291K using a Rigaku Saturn724 CCD diffractometer equipped with a graphite-monochromatized Mo*Kα* radiation [λ = 0.71073 Å] using OMEGA scans. Data collection and reduction were performed and the unit cell was initially refined by using CrystalClear -SM Expert 2.0 r$^2$ software. The structure was solved by direct methods and refined by least squares method on $F^2$ using SHELXTL-97 system of programs. Data for **C4** and **2** were carried out at 291 K on a Bruker Smart Apex CCD area detector equipped with a graphite monochromated MoKα radiation (λ= 0.71073 Å). The absorption correction for all complexes was performed using SADABS. All the structures were solved by direct methods and refined employing full-matrix least-squares on $F^2$ by using SHELXTL (Bruker, 2000) program and expanded using Fourier techniques. All non-H atoms of the complexes were refined with anisotropic thermal parameters. The hydrogen atoms were included in idealized positions. The hydrogen atom of $H_2O$ cannot be found from the difference FFT graph, Due to the $H_2O$ molecules are in disordered (share of non integer), So that the hydrogen atom of $H_2O$ are added by the theoretical hydrogenation and the O-H bond lengths are fixed at 0.85 angstroms and H-O-H angles are fixed to 109 degrees. This manuscript did not discuss hydrogen bond because the hydrogen bond here is meaningless. Final residuals along with unit cell, space group, data collection, and refinement parameters are presented in Table S1.

**Experimental Section:**

**Self-assembly of dimetallic corners.**

**{[(bpy)Pd]$_2$L$_2$}(NO$_3$)$_2$ (C1)** (bpy)Pd(NO$_3$)$_2$ (19.33mg, 0.05mmol) was added to a suspension of HL (7.2mg, 0.05mmol) in D$_2$O (1mL), and the mixture was stirred for 12 h at room temperature. The mixture was filtered and the resulting clear deep yellow solution was evaporated to give a yellow crystal. Yield: 22.2mg(94.87%). $^1$H NMR (400 MHz, D$_2$O, Si(CH$_3$)$_4$ as external standard , 25 $^o$C, ppm): 8.64 (s, 4H, pz-H), 8. 45 (d, J=6.8Hz, 4H, py-H), 8.37 (d, 4H, J=8.0 Hz, bpy-H), 8.29 (t, J=7.68 Hz,8.12 Hz, 4H, bpy-H), 8.22 (d, J=5.36Hz, 4H, py-H), 8.03 (d, J=6.88Hz, 4H, bpy-H). X-ray quality crystals were grown by the slow evaporation of a aqueous solution of **C1** at room temperature.

The PF6 salt of **C1** was obtained by adding a ten-fold excess of KPF$_6$ to its aqueous solution at 60°C, which resulted in the immediate deposition of **C1a** as yellow microcrystals in quantitative yield. The crystals were filtered, washed with minimum amount of cold water and dried. ESI-MS (CH$_3$CN) *m/z*: 959.02[**C1a**-PF$_6^-$ ]$^{1+}$, 407.02[**C1a**-2PF$_6^-$]$^{2+}$.

**{[(bpy)Pt]$_2$L$_2$}(NO$_3$)$_2$ (C2).** (bpy)Pt(NO$_3$)$_2$ (23.8mg, 0.05mmol) was added to a suspension of HL[1] (7.2mg, 0.05mmol) in H$_2$O (2mL) and the mixture was stirred for 12 h at 100℃. Then adding K$_2$NO$_3$ to the system and continuing to stir for 24h at 100℃. The mixture was filtered and the resulting clear yellow solution was evaporated to give a light yellow crystal. Yield: 25.2mg(87.5%)$^1$H NMR (400 MHz, D$_2$O, Si(CH$_3$)$_4$ as external standard , 25 $^o$C, ppm): 8.62 (s, 4H, pz-H), 8.48 (d, J=6.52Hz, 4H,py-H), 8.37 (d, J=5.72Hz, 4H,bpy-H), 8.31-8.25 (m, 8H, bpy-H), 7.98 (d, 4H , J=6.04Hz, py-H), 7.55(t, J=6.76Hz,6.28Hz, 4H, bpy-H).

The PF6 salt of **C2** was obtained by adding a ten-fold excess of KPF$_6$ to its aqueous solution at 60°C, which resulted in the immediate deposition of **C2a** as yellow microcrystals in quantitative yield.

The crystals were filtered, washed with minimum amount of cold water and dried. ESI-MS ($CH_3CN$) *m/z*: 1132.8 [**C2a**-$PF_6^-$ ]$^{1+}$, 493 [**C2a**-2$PF_6^-$]$^{2+}$.

**{[(ppy)Pt]$_2$L$_2$} (C3).** A mixture of [(ppy)$PtCl_2$]($Bu_4N$) (124 mg, 0.175 mmol), HL (76.3 mg, 0.3mmol), Ag($CF_3SO_3$) and NaOMe as base in $CH_3CN/CH_3OH$ (1:1 v/v) was heated at 40℃ under a nitrogen atmosphere for 3 days. The orange suspension gradually became a clear green-orange solution and was allowed to cool to room temperature. Then the solvent was evaporated to 5 mL. Addition of diethyl ether yielded an orange microctystal. Yield: 72.5 mg, 88.25%. MALDI-MS($CH_2Cl_2$): *m/z* 986.6 [**C3**] ，841.1 [**C3** –HL$^1$].

**{[(bpy)Pd]$_2$L´$_2$}($NO_3$)$_2$ (C4).** (bpy)Pd($NO_3$)$_2$ (19.33mg, 0.05mmol) was added to a suspension of HL´ (8.6mg, 0.05mmol) in $D_2O$ (1mL), and the mixture was stirred for 12 h at room temperature. The mixture was filtered and the resulting clear deep yellow solution was evaporated to give a yellow crystal. Yield: 22.0mg(86.25%). $^1$H NMR (400 MHz, $D_2O$, Si($CH_3$)$_4$ as external standard , 25 $^o$C, ppm): 8.69 (d, J=6.6Hz, 4H, py-H), 8.56 (d, J=8.12Hz, 4H, py-H), 8.28 (t, 4H, $J_1$=7.76Hz, $J_2$=7.12 Hz, bpy-H), 8.06 (d, J=5.08 Hz, 4H, bpy-H), 7.90 (d, $_1$=6.76Hz, 4H, bpy-H), 2.5 (s, 12H, CH3). X-ray quality crystals were grown by the slow evaporation of a aqueous solution of **C4** at room temperature.

**Self-assembly of Metallic Macrocycles.**

**{[(bpy)Pd]$_6$L$_4$}($NO_3$)$_8$ (1).** (bpy)Pd($NO_3$)$_2$ (9.70mg, 0.025mmol) was added to a suspension of **C1** (23.43mg, 0.025mmol) in $D_2O$ (1mL), and the mixture was stirred for 24 h at at 100℃. The mixture was filtered and the resulting clear deep yellow solution was evaporated to give a yellow crystal. Yield: 58mg(87.6%). 1H NMR (400 MHz, $D_2O$, Si($CH_3$)$_4$ as external standard , 25$^o$C, ppm): 9.02 (d, J=6.48Hz, 8H, py-H), 8.58 (s, 8H, pz-H), 8.58-8.48 (t, 12H, bpy-H), 8.42-8.38(m, 12H, bpy-H), 8.30(d, J=5.48Hz, 8H, py-H), 7.88 (d, J=6.6Hz, 8H, bpy-H), 7.72 (t, J=6.92Hz,6.64Hz, 8H, bpy-H), 7.66 (t, J=7Hz,6.56Hz, 4H, bpy-H), 7.56 (d, J=5.52Hz, 4H, bpy-H). X-ray quality crystals were grown by the slow evaporation of a aqueous solution of **1** at room temperature.

The PF6 salt of **1** was obtained by adding a ten-fold excess of $KPF_6$ to its aqueous solution at 60°C, which resulted in the immediate deposition of **1a** as yellow microcrystals in quantitative yield. The crystals were filtered, washed with minimum amount of cold water and dried. ESI-MS (acetonitrile) *m/z*: 959.02 [**1a**-3$PF_6^-$ ]$^{3+}$.

**{[(bpy)Pt]$_4$[(bpy)Pd]$_2$L$_4$}($NO_3$)$_8$ (2).** (bpy)Pd($NO_3$)$_2$ (9.7mg, 0.025mmol) was added to a suspension of **C2** (27.87mg, 0.025mmol) in $D_2O$ (2mL) for 24 h at 100℃. The mixture was filtered and the resulting clear yellow solution was evaporated to give a yellow crystal. Yield: 32mg(86.5%). $^1$H NMR (400 MHz, $D_2O$, Si($CH_3$)$_4$ as external standard, 25$^o$C, ppm): 9.15 (d, J=6.04Hz, 8H, py-H), 8.78 (s, 8H, pz-H), 8.57(t, J=7.96Hz, 5.64Hz, 12H, bpy-H), 8.50(t, J=7.6Hz, 8.52Hz,12H, bpy-H), 8.44(t, J=7.8Hz, 8.6Hz, 8H, py-H), 7.99 (d, J=5.76Hz, 8H, bpy-H), 7.83 (m, J=6.36Hz, 6.76Hz, bpy-H), 7.72(t, J=5.96Hz, 7.12Hz, 4H, bpy-H), 7.61 (d, J=5.44Hz, 4H, bpy-H). X-ray quality crystals were grown by the slow evaporation of a aqueous solution of **2** at room temperature.

The PF6 salt of **2** was obtained by adding a ten-fold excess of $KPF_6$ to its aqueous solution at 60°C, which resulted in the immediate deposition of **2a** as yellow microcrystals in quantitative yield. The crystals were filtered, washed with minimum amount of cold water and dried. ESI-MS (acetonitrile) *m/z*: 667.8 [2**a**-3$PF_6^-$ ]$^{3+}$.

## NMR and MS spectra

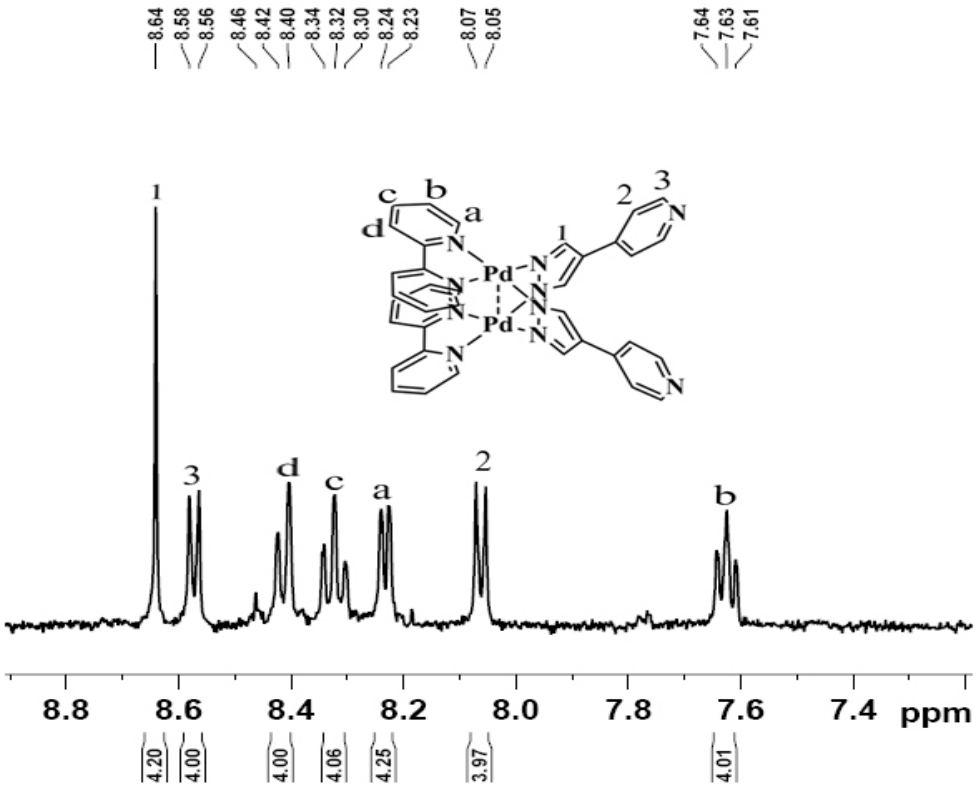


**Fig S1**. $^{1}$H NMR spectrum of **C1** in $D_2O$

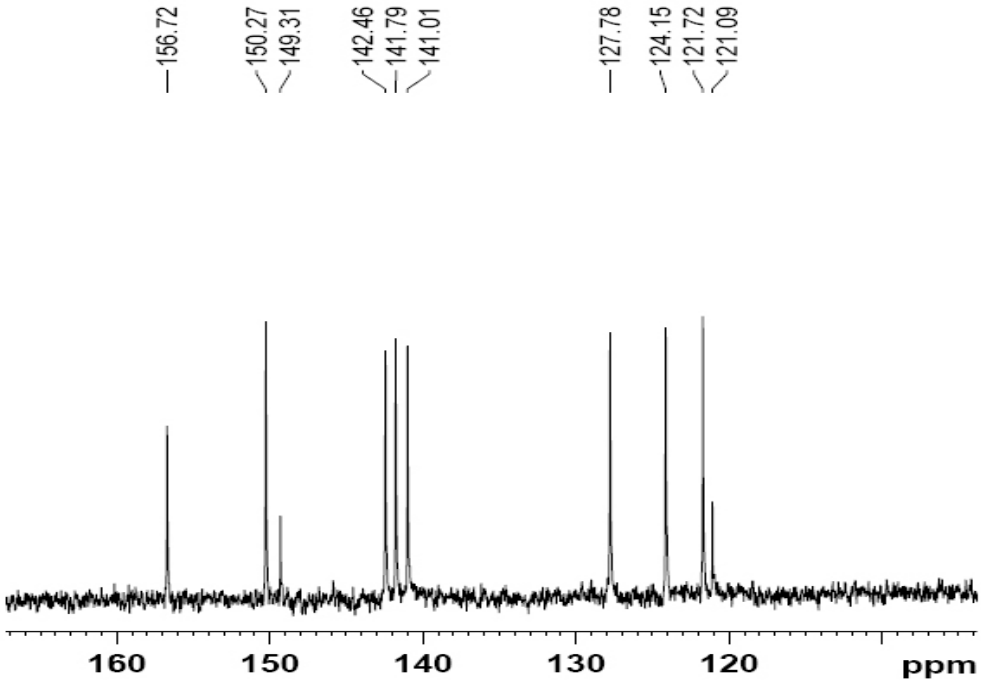


**Fig S2**. $^{13}$C NMR spectrum of **C1** in $D_2O$

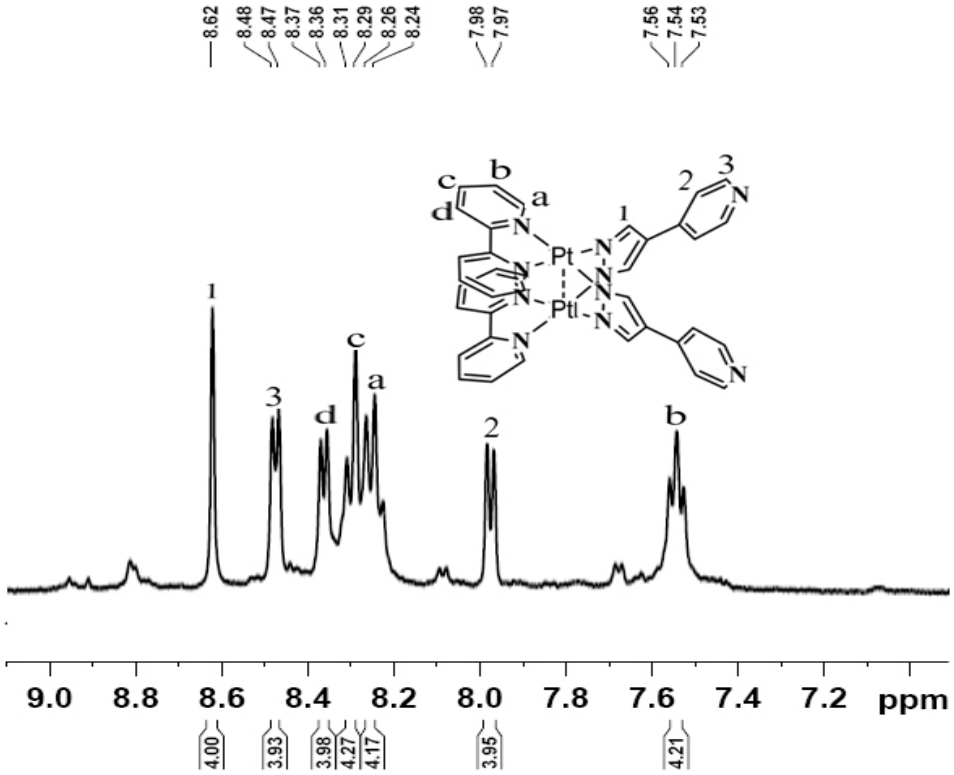


**Fig S3**. $^{1}$H NMR spectrum of **C2** in $D_2O$

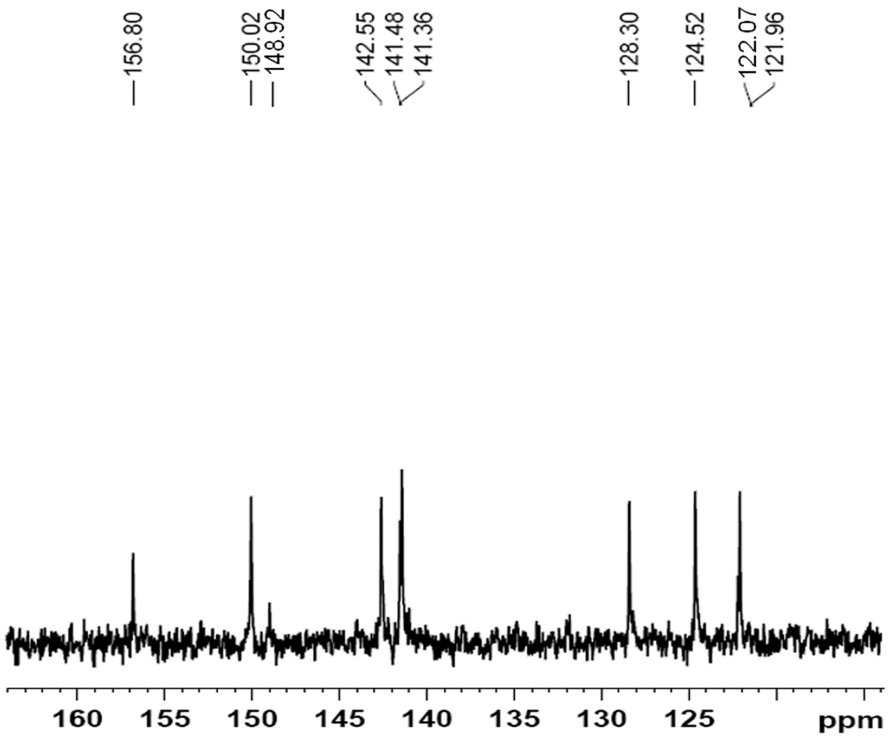


**Fig S4**. $^{13}$C NMR spectrum of **C2** in $D_2O$

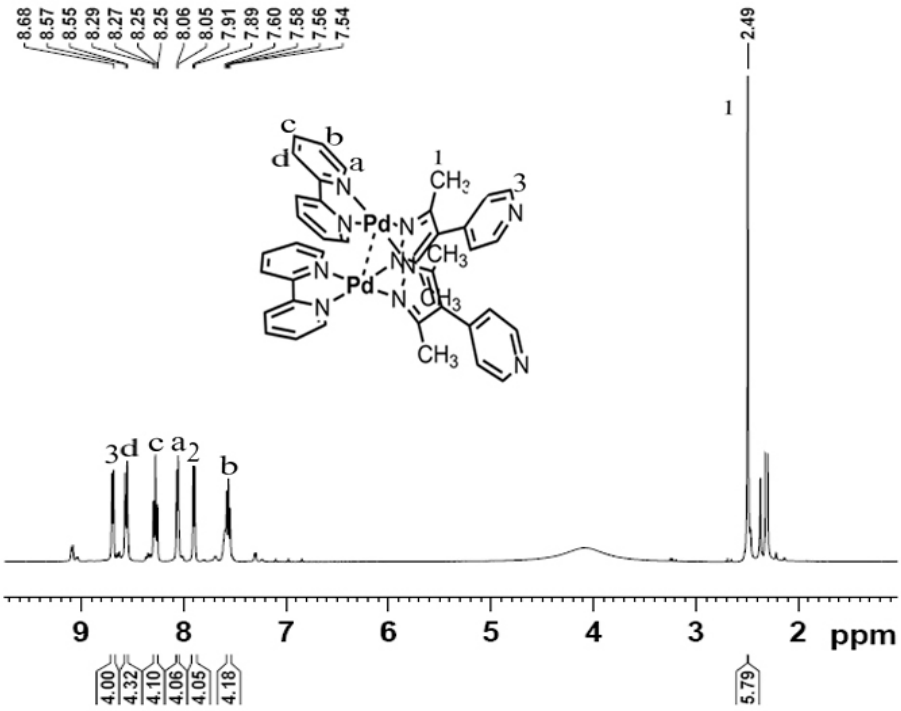


**Fig S5**. $^{1}$H NMR spectrum of **C4** in $D_2O$

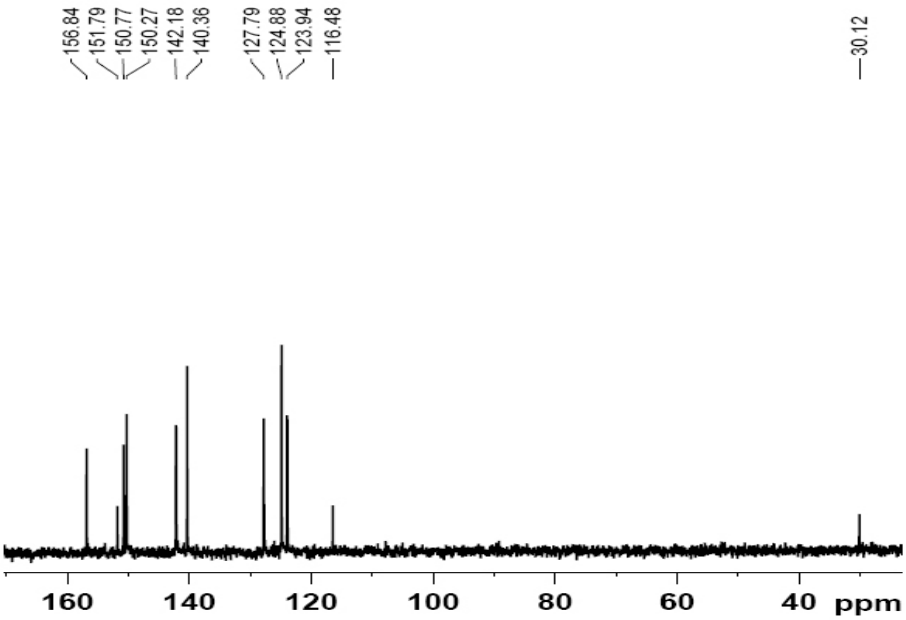


**Fig S6**. $^{13}$C NMR spectrum of **C4** in $D_2O$

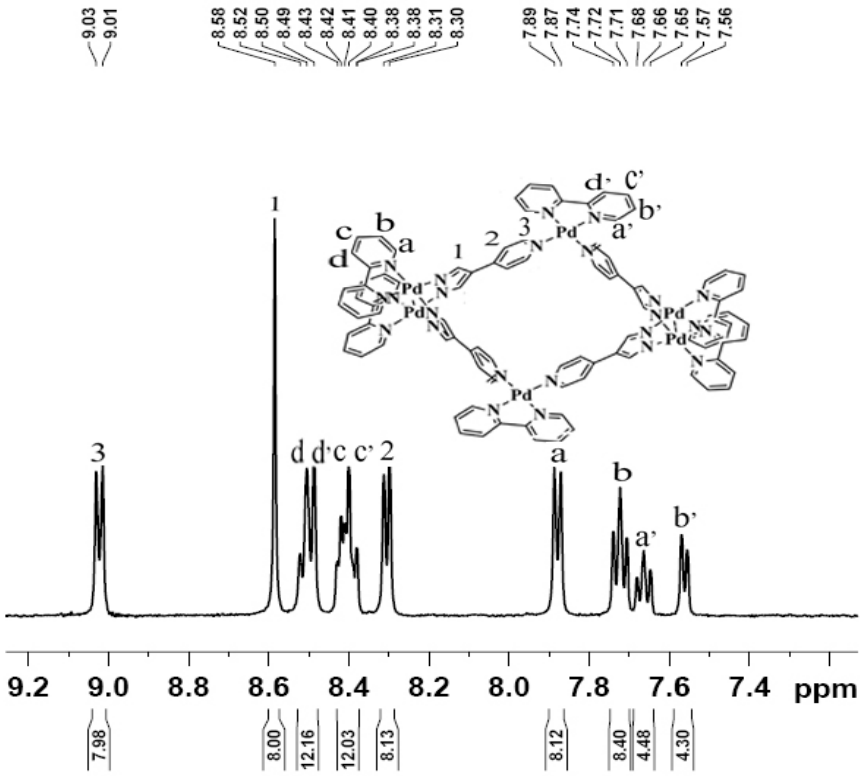


**Fig S7**. $^{1}$H NMR spectrum of **1** in $D_2O$

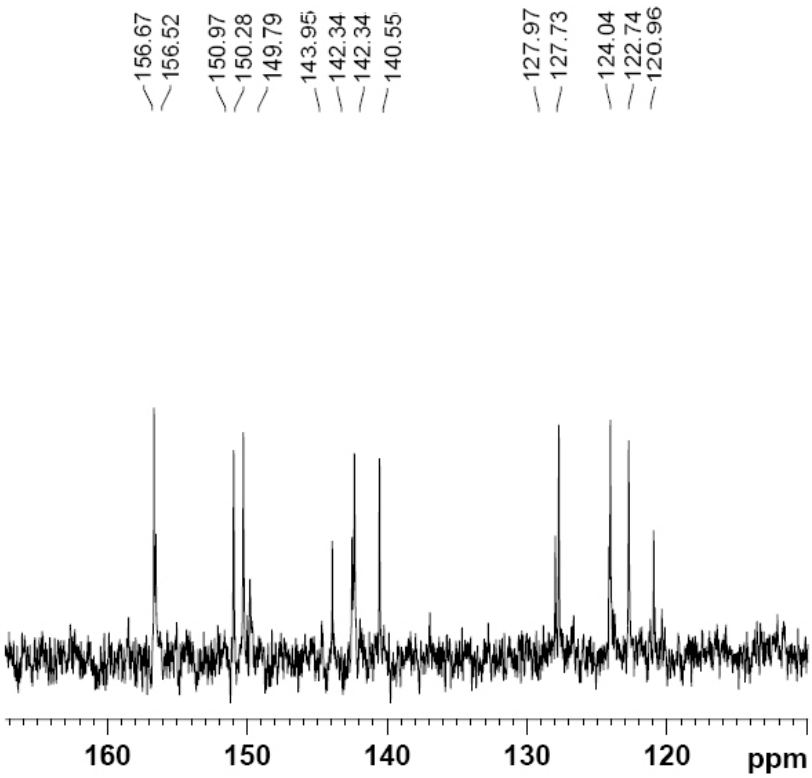


**Fig S8**. $^{13}$C NMR spectrum of **1** in $D_2O$

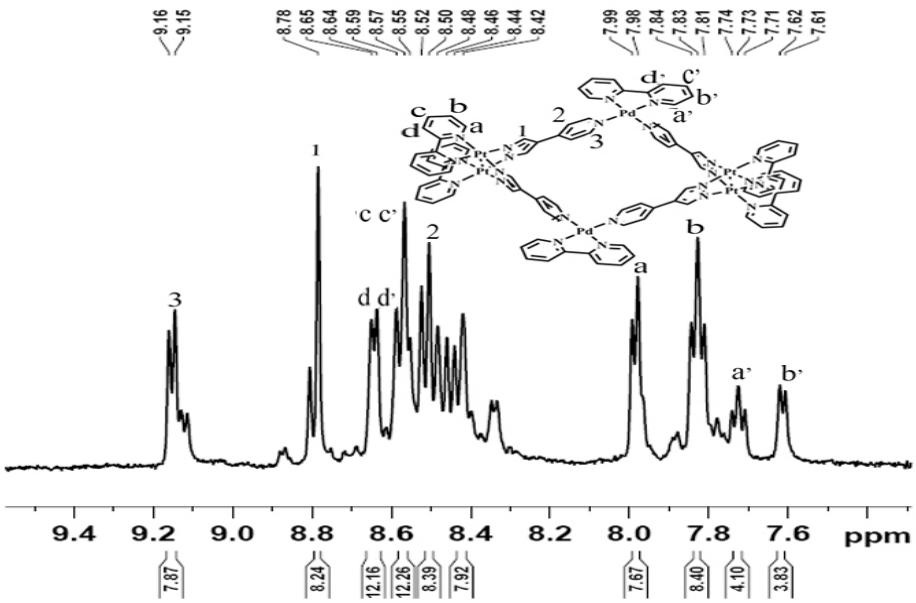


**Fig S9.** $^{1}$H NMR spectrum of **2** in $D_2O$

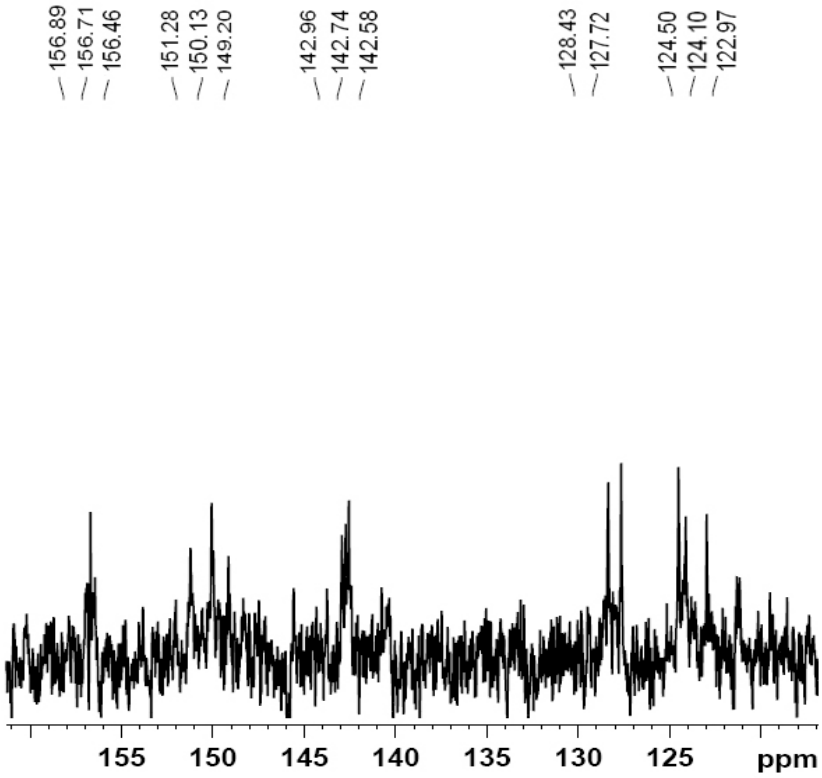


**Fig S10**. $^{13}$C NMR spectrum of **2** in $D_2O$

## Analysis of the NMR spectra

All of $^{1}H$ NMR spectra for the self-assembled complexes showed sets of high resolution signals. From the Figure S1, S3 and S5 we could find that the dimetallic clips **C1, C2** and **C4** were formed as the pure products and no any other products founded at all in $D_2O$ at room temperature, the proton at 2,2'-bipyridine (bpy) and L showed only one group of the single peaks each other. Compared with the dimetallic clips, the protons at pyridine coordinated to (bpy)M centers of all the metallomacrocycllic complexes had obvious shift toward downfield due to the deshielding effect of metal ions. Furthermore, the proton signals at bpy in the monometal unit were founded that were different from the dimetal unit, which meant the bpy groups in the monometal and dimetal centers were in two different chemical environments.

In addition, there appeared five peaks in the $^{13}C$ NMR of all the macrocycles, compared to the dimetallic corners respectively.

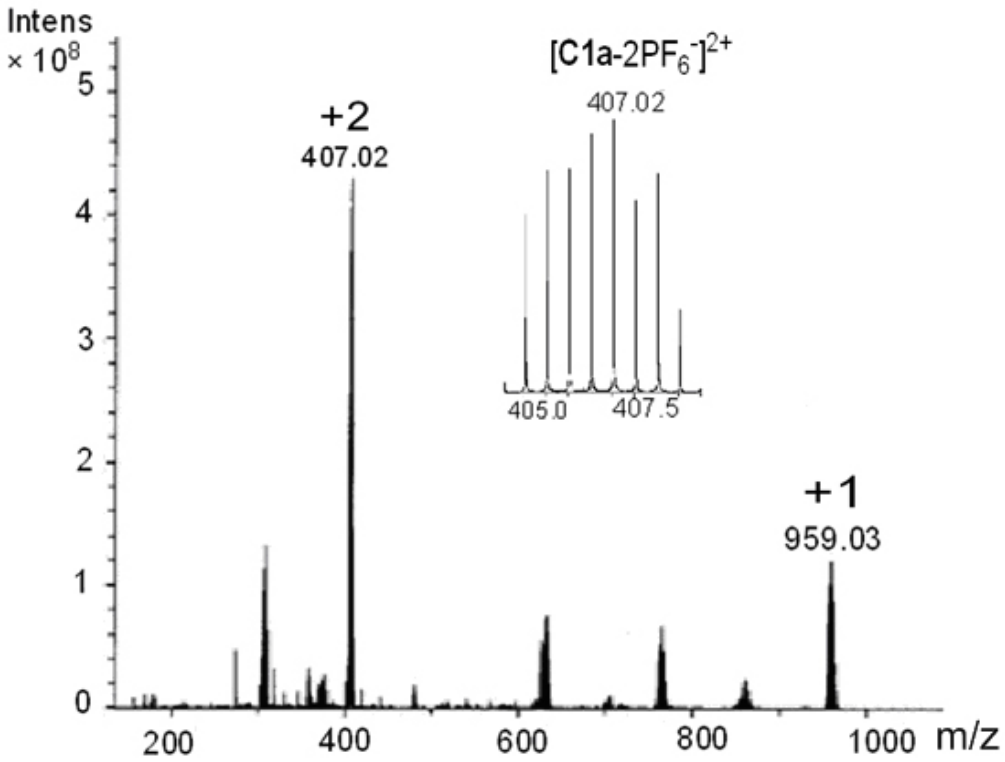


**Fig S11.** ESI-MS spectrum of **C1a** in acetonitrile. The inset shows the isotopic distribution of the species [**C1a**-2$PF_6^-$]$^{2+}$.

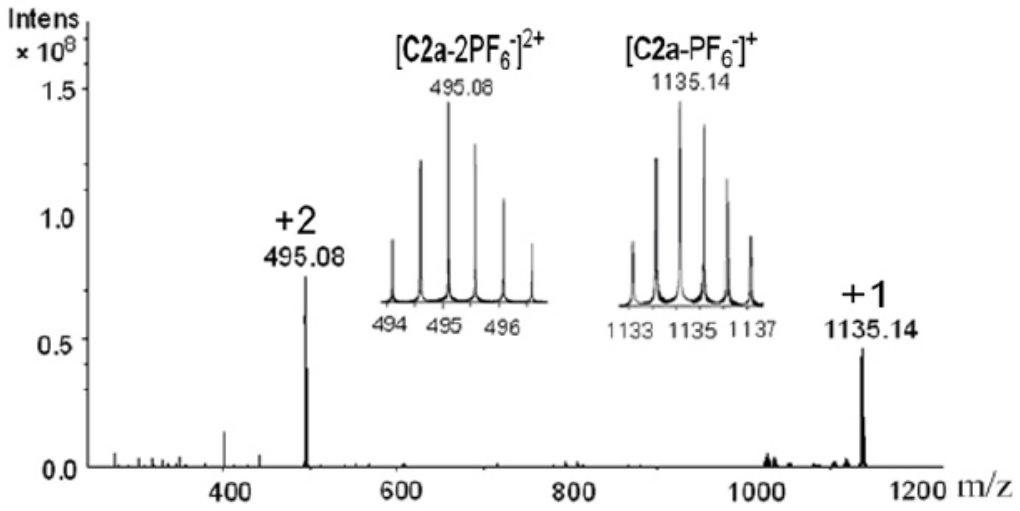


**Fig S12.** ESI-MS spectrum of **C2a** in acetonitrile. The inset shows the isotopic distribution of the species [**C2a**-2$PF_6^-$]$^{2+}$ and [**C2a** -$PF_6^-$]$^{1+}$.

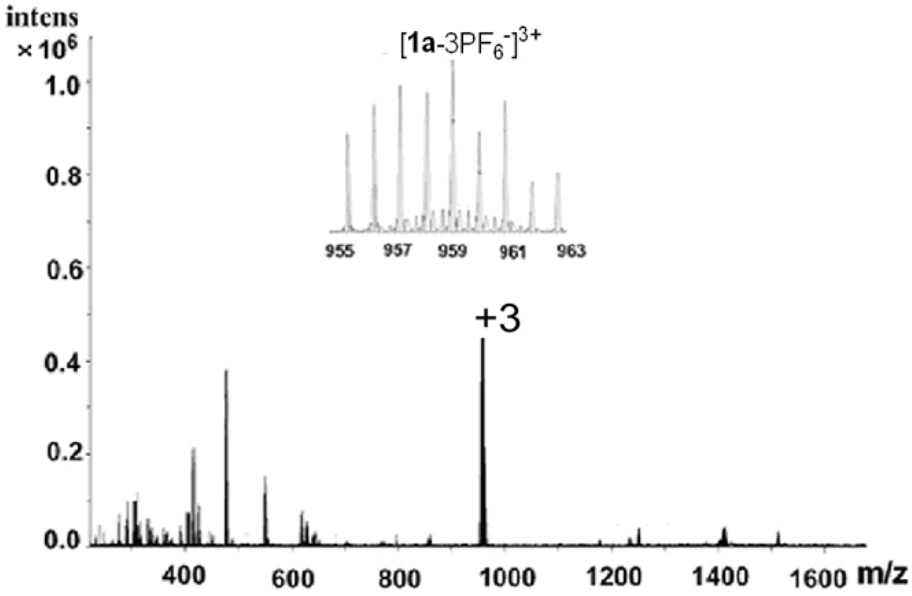


**Fig S13.** ESI-MS spectrum of **1a** in acetonitrile. The inset shows the isotopic distribution of the species [**1a**-3$PF_6^-$]$^{3+}$.

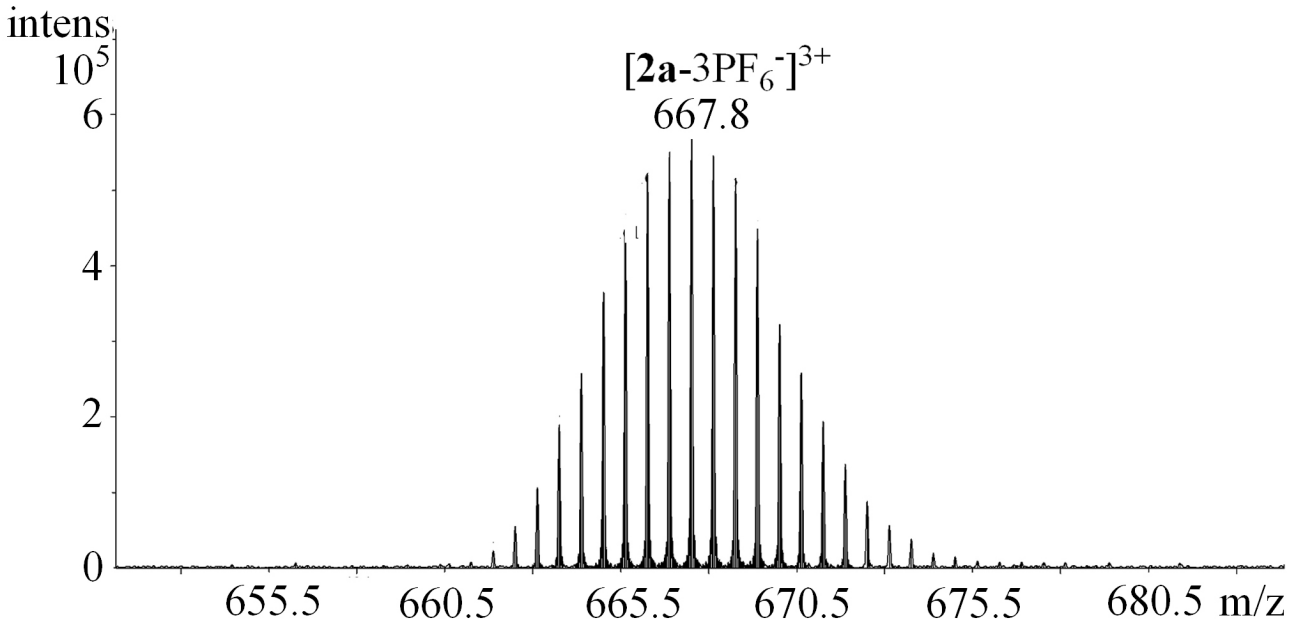


**Fig S14.** ESI-MS of **2a** in acetonitrile. The inset shows the isotopic distribution of the species [**2a**-3$PF_6$-]$^{3+}$.

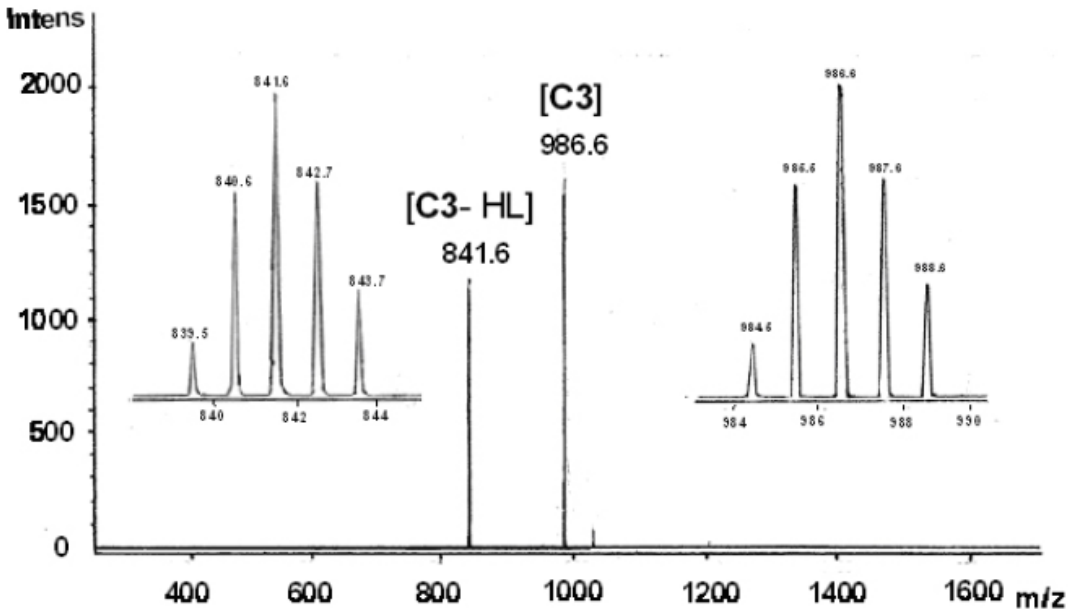


**Fig S15**. MALDI-TOF of **C3** in acetonitrile.The inset shows the isotopic distribution of the species[C3] and [C3-HL1].

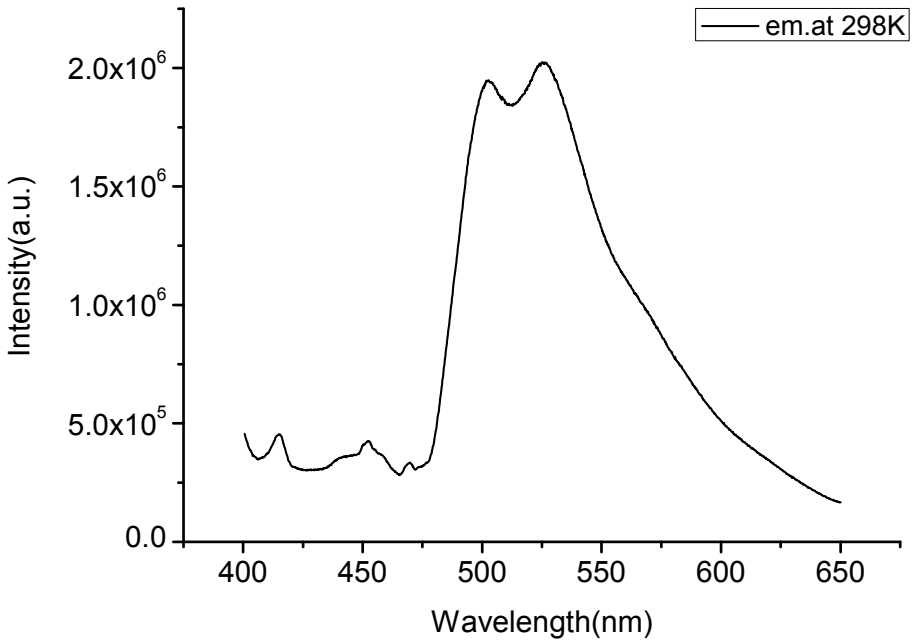


**Fig S16.** Solid state emission spectra of {[(ppy)Pt]2L2}(C3) at 298 K. (Excitation λ=370 nm.)

**Tab S1** Selected Bond Distances (Å) and Angles (°) for Complexes **C4**, **1** and **2**.

$[(bpy)_2Pd_2\mathbf{L}_2](NO_3)_2$ (**C4**)

| | | | |
|---|---|---|---|
| Pd1–Pd2 | 3.082(11) | Pd1–N(5) | 2.010(3) |
| Pd1–N(8) | 2.024(3) | Pd2–N(6) | 2.027(3) |
| Pd2–N(9) | 1.996(3) | | |
| N(9)–Pd2–N(6) | 84.94(12) | | |
| N(8)–Pd1–N(5) | 86.70(12). | | |

$\{[(bpy)_2Pd_2]_2[(bpy)Pd]_2\mathbf{L}^1{}_4\}NO_3)_8$ (**1**)

| | | | |
|---|---|---|---|
| Pd(1)–Pd(2) | 3.432(4) | Pd(1)–N(7) | 1.988(3) |
| Pd(1)–N(10) | 1.984(4) | Pd(2)–N(8) | 1.981(4) |
| Pd(2)–N(11) | 1.992(3) | Pd(3)–N(9) | 2.000(4) |
| Pd(3)–N(12A) | 1.985(3) | | |
| N(7)–Pd(1)–N(10) | 85.88(13) | | |
| N(8)–Pd(2)–N(11) | 86.27 (14) | | |
| N(9)–Pd(3)–N(12A) | 87.64 (13) | | |

$\{[(bpy)_2Pt_2]_2[(bpy)Pd]_2\mathbf{L}^1{}_4\}NO_3)_8$ (**2**)

| | | | |
|---|---|---|---|
| Pt(1)–Pt(2) | 3.161 (5) | Pd(1)–N(7) | 2.000(6) |
| Pd(1)–N(10) | 2.011(6) | Pt(1)–N(11A) | 1.988(7) |
| Pt(1)–N(6) | 1.988(5) | Pt(2)–N(5) | 1.951(6) |
| Pt(2)–N(12) | 1.998(6) | | |
| N(7)–Pd(1)–N(10) | 85.4(2) | | |
| N(6)–Pt(1)– N(11A) | 84.7(3) | | |
| N(5)–Pt(2)–N(12A) | 86.1(2) | | |

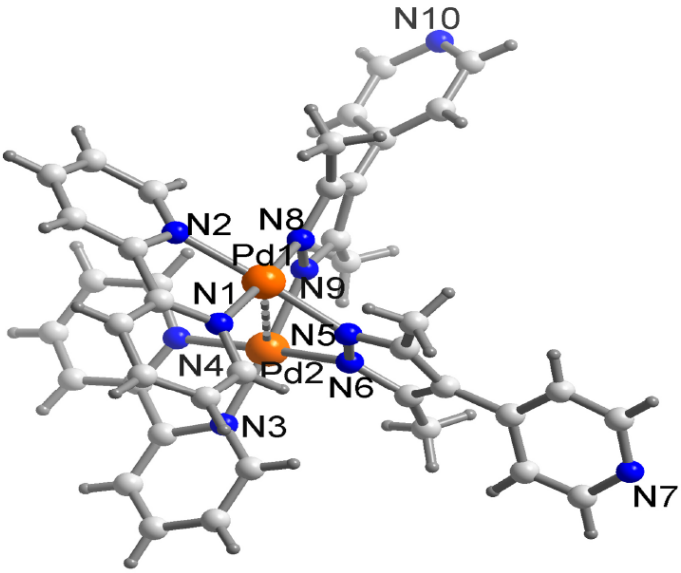


**Fig S17.** Crystal structure of **C4**(free anions and solvent molecules were omitted for clarity).

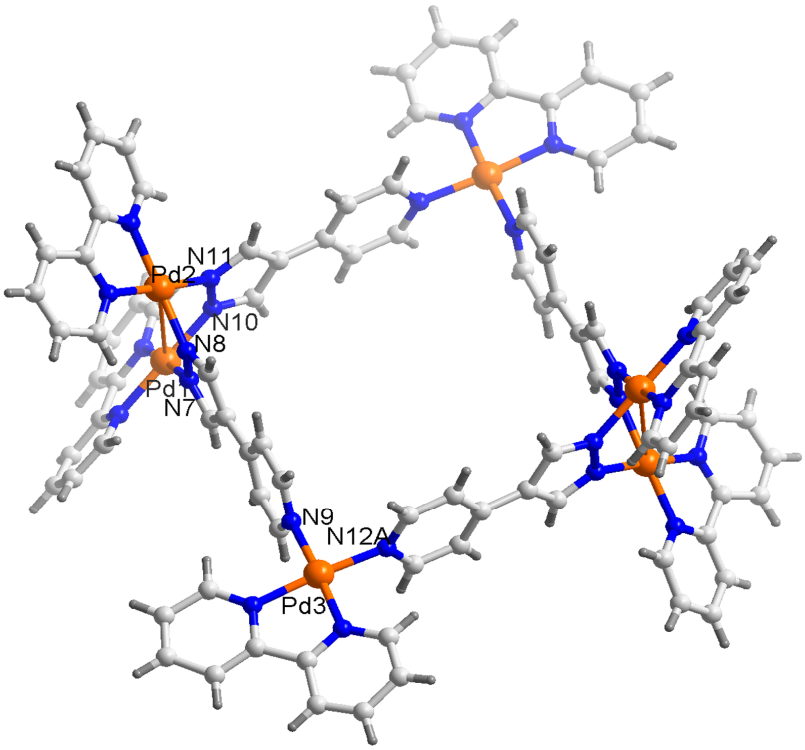


**Fig S18.** Crystal structure of **1**(free anions and solvent molecules were omitted for clarity).

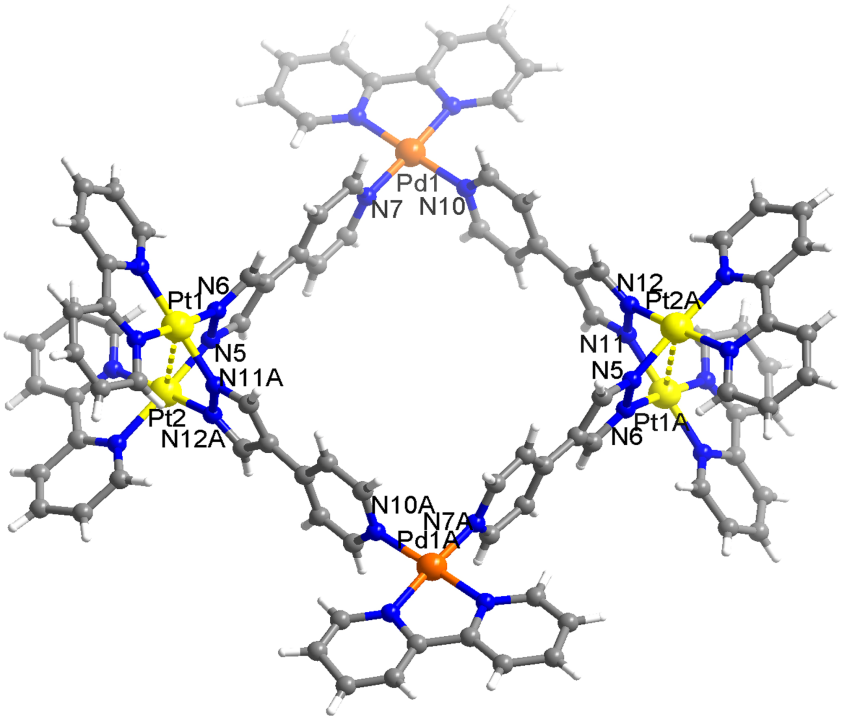


**Fig S19.** Crystal structure of **2**(free anions and solvent molecules were omitted for clarity).

## The analysis of crystal structures

In the structure of **C4**·2$H_2O$, the distances of the Pd…Pd bond in the same molecular are 3.082 Å and is in the range of typical Pd···Pd interactions (2.60−3.30 Å). The torsion angle between THE pyridyl-pyrazole fragments (planes N5−N6 and N8−N9) is 87°. Based on these data, the shape of the complex at the first process during the self-assembly is clip-liked.

In the structure of **1**•10$H_2O$, which resides on a crystallographic inversion center, the Pd3–Pd3A diagonal is 14.892Å whereas the diagonal defined by the midpoints of the two $Pd_2$ units is 13.512 Å. The vertex angles subtended by the $Pd_2$ units are less than the ideal value of 90° [N(7)–Pd(1)– N(10) 85.88°, N(8)–Pd(2)–N(11) 86.27°], a situation that leads to a bending of the pyridyl-pyrazole ligands to accommodate ring closure. There is also dimetal interaction based on the Pd(1)–Pd(2) separated at 3.432 Å, which is lomgerer than the separations Pd···Pd interactions(2.60−3.30 Å) reported in our former work.

In the structure of **2**•8$H_2O$ the Pd1–Pd1A diagonal is 15.122 Å whereas the diagonal defined by the midpoints of the two $Pt_2$ units is 13.590 Å. The vertex angles subtended by the $Pt_2$ units are less than the ideal value of 90° [N(6)–Pt(1)– N(11A) 84.7(3), N(5)–Pt(2)–N(12A) 86.1(2)], a situation that leads to a bending of the pyridyl-pyrazole ligands to accommodate ring closure. There is also dimetal interaction based on the Pt(1)–Pt(2) separated at 3.161 Å, which is shorter than the separations Pt···Pt interactions(3.372−3.349 Å) reported in our former work.

**Table S2.** Summary of crystallography data collection and structure refinement for compounds **C4**, **1** and **2**.

| | **C4**·2$H_2O$ | **1**·10$H_2O$ | **2**·8$H_2O$ |
|---|---|---|---|
| formula | $C_{40}H_{40}N_{10}O_2Pd_2$ | $C_{92}H_{92}N_{24}O_{10}Pd_6$ | $C_{92}H_{88}N_{24}O_8Pt_4Pd_2$ |
| FW | 1038.65 | 2332.30 | 3147.10 |
| crystal size [mm] | 0.20 x 0.22 x 0.28 | 0.22 x 0.24 x 0.30 | 0.24 x 0.26 x 0.28 |
| crystal system | Triclinic | Triclinic | Triclinic |
| space group | P-1 | P-1 | P-1 |
| *a* [Å] | 13.397(3) | 12.6289(6) | 15.2067(15) |
| *b* [Å] | 16.610(3) | 16.3546(8) | 15.8034(16) |
| *c* [Å] | 22.29(4) | 17.1424(6) | 17.2256(19) |
| *α* [°] | 86.15(3) | 75.019(1) | 116.487(2) |
| *β* [°] | 89.18(3) | 86.462(2) | 102.313(4) |
| *γ* [°] | 89.19(3) | 77.091(1) | 96.752(2) |
| *V* [$Å^3$] | 4936.5(17) | 3333.8(3) | 3511.2(6) |

| Z | 2 | 1 | 1 |
|---|---|---|---|
| $\rho_{calcd}$, [g/cm$^{-3}$] | 1.398 | 1.162 | 1.488 |
| μ [mm$^{-1}$] | 0.787 | 0.842 | 4.292 |
| $F$(000) | 2100 | 1168 | 1524 |
| $2\theta_{max}$ [°] | 52.00 | 52.00 | 52.00 |
| no. unique data | 19403 | 13113 | 13629 |
| parameters | 1206 | 685 | 808 |
| GOF [F$^2$][a] | 1.03 | 1.07 | 1.08 |
| R [$F^2$>2σ($F^2$)], wR[$F^2$][b] | 0.1115, 0.1093 | 0.1097, 0.1026 | 0.1127, 0.1073 |
| $\Delta\rho_{max}$, $\Delta\rho_{min}$ [e Å$^{-3}$] | 0.72, -1.52 | 0.45, -0.36 | 1.42, -1.43 |

[a] GOF = $[w(F_o^2 - F_c^2)^2]/(n - p)^{1/2}$, where $n$ and $p$ denote the number of data points and the number of parameters, respectively. [b] R1 = $(||F_o| - |F_c||)/|F_o|$; wR2 $=[w(F_o^2 - F_c^2)^2]/[w(F_o^2)^2]^{1/2}$,Where $w=1/[\sigma^2(F_o^2)+(aP)^2+bP]$ and $P=(F_o^2+2F_c^2)/3$.

## Reference

(1) Armarego, W. L. F.; Perrin, D. D. *Purification of Laboratory Chemicals*, 4$^{th}$ed; Butterworth Heinemann; Oxford, **1997**.

(2) Mulyana, Y.; Kepert, C. J.; Lindoy, L. F.; Parkin , A.; Turner , P. *DaltonTrans.* **2005** , 1598-1601.